

CHAPTER 3

Micro-structural Investigations on Oppositely Charged Mixed Surfactant Gels with Potential Dermal Applications

ABSTRACT

Dicarboxylic amino acid-based surfactants (N-dodecyl derivatives of -amino malonate, -aspartate, and -glutamate) have been combined with hexadecyltrimethylammonium bromide (HTAB) form a variety of aggregates. Composition and concentration dependent mixtures exhibit liquid crystal, gel, precipitate and clear isotropic solutions. Liquid crystalline patterns were identified by polarization optical microscopy and fluorescence microscopy. FE-SEM studies reveal porous and flower like morphology. Phase transitions, along with weight loss, depend on composition where thermotropic behaviors were revealed through thermogravimetry and differential scanning calorimetric analyses. Systems comprising more than 60% HTAB demonstrate shear thinning behavior. Gels cause insignificant toxicity to human peripheral lymphocytes and irritation to mouse skin. Also they do not display the symptoms of cutaneous irritation, neutrophilic invasion and inflammation (erythema, edema, and skin thinning). Such gels exhibit antibacterial effect on *Staphylococcus aureus*, a potent causative agent of skin and soft tissue infections, suggesting its possible application as vehicle for dermatological drug delivery.

Scientific Reports, 2021, 11, 1-9

DOI: 10.1038/s41598-021-94777-2

1. INTRODUCTION

Formation of gels and different liquid crystalline phases by oppositely charged mixed surfactant systems depend on composition, surfactant chain length, salinity, temperature, pH and external field, *etc.*^{122, 227-230} Artificial gels possess regulated super structure where the properties of the fabricated liquid crystals,^{177-178,192,231-232} depend on electrostatic, hydrophobic, hydrogen bond, and van der Waals interactions among the components.²⁻⁴ Gels are associated with two independent transitions, *viz.*, sol-gel transition of the gelator and isotropic-anisotropic transition of liquid crystals.^{131, 231-236} Mesogens in liquid crystals remain in fashioned order and fluid state; can have different shapes. Rod shaped mesogens exhibit nematic and smectic phase while disk shaped mesogens show columnar phase.^{131, 233} Gelatinous property of surfactant aggregates largely depends on the molecular architecture of the aggregating species that control its structure and shape.^{233, 237, 238}

Gels have versatile applications in tissue engineering,¹³⁸ hemostasis bandages,^{125,128,139,239,240} photo patterning,^{140, 235, 241-243} 3D-printing,^{141, 244} electrochemistry,¹⁴² pharmaceutical formulation,^{230, 245-247} and regenerative medicine,^{143, 232, 248, 249} *etc.* Recent advances in the design and synthesis of dicarboxylic amino acid based surfactants (C₁₂AAS)Na₂ have different versatile applications as chelator in metal extraction.¹²⁴ However due to its “green nature” the present research groups studied its aggregation behavior with HTAB where some mixed surfactant formed gel. This has instigated to undertake further investigations on such aggregates at higher concentration with the aim in using them as novel dermatological drug delivery systems.

The main aim of the present work is physicochemical investigations on different types of aggregates that formed by (C₁₂AAS)Na₂+HTAB. While HTAB exhibits antimicrobial activities, however, (C₁₂AAS)Na₂ are biocompatible. Because of its toxicity, individual use of HTAB is unwarranted. However, when HTAB is used in combination with (C₁₂AAS)Na₂, its toxicity is expected to get substantially reduced. To check the biocompatibility of gels and its possible dermatological application,

cytotoxicity, skin irritation and histological studies were carried out. Besides antibacterial activity on *Staphylococcus aureus*, causative factor for persistent skin and tissue infections.

2. EXPERIMENTAL SECTION

2.1. Materials. Hexadecyltrimethylammonium bromide (HTAB) and histopaque-1077TM were from Sigma-Aldrich Chemicals Pvt. Ltd. (USA). Phenol, haematoxylin, eosin Y and 3-(4,5-dimethylthiazol-2-yl)-2,5-diphenyl tetrazolium bromide (MTT) were purchased from HiMedia Laboratories Pvt. Ltd. India while rhodamine-B and fluorescein were from Sisco Research Laboratory Pvt. Ltd. India. Double distilled water was used throughout the experiments. The 99% pure chemicals were used for different experimental studies and were used as received.

2.2. Methods.

2.2.1. Phase manifestation. Composition of different phases can be assessed by analyzing the ratio of the stock solutions of the constituent surfactants. Accurate boundary of two phase region were obtained by stepwise adding higher concentration of $(C_{12}AAS)Na_2$ into the HTAB solution using a calibrated micropipette under constant stirring. On the basis of visual observation, more than one hundred samples were collected at different $(C_{12}AAS)Na_2$ and HTAB weight ratio that clearly identified phase boundaries.¹³⁰ The experiment was repeated thrice to check the reproducibility.

2.2.2. Polarization optical microscopy (POM) studies. Texture of different combinations of the mixed surfactant systems were recorded with a polarization optical microscope (Nikon ECLIPSELV100POL, Japan) set with a CCD camera. Sample was placed on to a glass slide and thereafter the POM images were recorded.

2.2.3. Fluorescence microscopic (FM) studies. Mixtures of $(C_{12}AAS)Na_2$ +HTAB at different combinations were also investigated with fluorescence microscopy doped with three sets of dyes: a) rhodamine B, b) eosin Y, and c) an equimolar mixture of rhodamine-B and eosin Y. Fluorescence images

were recorded with an upright microscope (NIKON ECLIPSE LV100POL, Japan) equipped with a green and red fluorescence active CCD camera (model no. DS-Fil).

2.2.4. Field emission scanning electronic microscopy (FE-SEM) studies. Morphology of the surfactant aggregates were studied using the scanning electron microscope (ZEISS EVO 18, Germany). Samples were prepared by drop casting the gel on a freshly cleaved mica foil and kept in air for two hours for solvent evaporation. They were further dried at reduced pressure for two hours. The gold sputtered samples were then analyzed for FE-SEM at the operating voltage of 20-30 kV.

2.2.5. Thermo gravimetric analysis (TGA). Weight loss and thermal decomposition of gels were investigated by TGA, was performed using Pyris 6 TGA-DTA-8000 (Perkin Elmer, USA). Samples were scanned in the temperature range of 50-500°C with a scan rate of 20°C min⁻¹ under nitrogen gas flow.

2.2.6. Differential scanning calorimetric (DSC) studies. DSC studies were performed to evaluate the chain melting temperature (T_m) and associated thermodynamic parameters of surfactant aggregates that control its physical states. DSC measurements were recorded using a Pyris 6 DSC-8000 (Perkin Elmer, USA) differential scanning calorimeter with indium as a calibrator before performing the experiment. Sample was equilibrated at 10 min then scanned in the temperature range 0-273°C with a scan rate of 10°C min⁻¹ during the heating cycle, while it was cooled at a scan rate of 5°C min⁻¹. Endothermic peak vs. temperature in evaluating different physicochemical parameter of mixed surfactant system were considered.²⁵⁰

2.2.7. Rheology studies. Rheology studies were done by a DV II-Pro rotoviscometer (Brookfield, USA) with a stated accuracy of ± 0.01 cP. 1.0 mL surfactant solutions of different concentrations (40, 60, 80 and 100 mm) were taken in a cone and plate type rotoviscometer.¹⁸⁹ Viscosities data were evaluated at different shear rate, ranging from 76-380 s⁻¹. Zero shear viscosity (η_0) was another important parameters that's were determined from the intercept of viscosity vs. shear rate plots.

2.3. Biological activities.

2.3.1. Cytotoxicity studies. Cytotoxicity studies were carried out following the method of Sun. et al.²⁵¹ 5 mL of human blood (volunteered by a healthy person) was diluted (1:1) with phosphate buffered saline (PBS) and added to Histopaque-1077. It was centrifuged at 1500 rpm for 40 min at room temperature. The upper monolayer containing lymphocytes was further washed through centrifugation. The lymphocytes were re-suspended in RPMI complete media supplemented with 10% (w/v) fetal bovine serum (FBS) and incubated for a day at 310K in a 5% (v/v) CO₂ environment (in CO₂ incubator).²⁵² Cytotoxicity of selected gels were estimated by MTT assay.²⁵³ 20 µL 5 % (w/v) MTT solution was added on microtitre plate, having RPMI-suspended lymphocytes. Experimental plate was incubated at 310K for 4 h in metabolizing MTT to formazan. The optical density (OD) of the samples are measured on ELISA reader (Model 550, BIO-RAD, USA) and percentage of cell viability can be calculated as:²⁵³

$$\text{Cell viability \%} = [\text{OD}_{\text{sample}} - \text{OD}_{\text{control}}] \times 100 / \text{OD}_{\text{control}} \quad (1)$$

2.3.2. Cutaneous irritation test. Cutaneous irritation test of selected gels were performed as mentioned in the Good Laboratory Practice Standards (GLPS) manual and the guidelines of Organization for Economic Co-operation and Development (OECD) for acute dermal irritation.²⁵¹ Thirty healthy swiss albino mice were divided into five groups, each group consisting six mice. Group A was set as negative control, treated with sterile distilled water and group B was positive control treated with 5% phenol water to develop skin irritation. Mice of group C, D and E were treated with 100 mM C₁₂MalNa₂+HTAB, C₁₂AspNa₂+HTAB and C₁₂GluNa₂+HTAB gels respectively. Before the test, the hairs of dorsal area of the trunk region of all the mice were removed and each applied topically with 500 µL of respective experimental gels and controls. After 4 h, any sign of erythema or edema in individual animal was recorded. This entire procedure of dermal application of gels and subsequent recording for any irritation was done for consecutive seven days.

2.3.3. Histological studies of mouse skin. After seven days of skin irritation study, all the animals were euthanized by carbon dioxide asphyxiation. The treated skins were processed in wax blocks and transverse sections were prepared, followed by staining with hematoxylin-eosinY (HE)²⁵⁴ and examined under light microscope (Axioscope A1; Carl Zeiss, Germany). The histology of gel-treated skins were compared with those of the control animals.

2.3.4. Antibacterial activity studies. Antibacterial efficacies of the gels against *Staphylococcus aureus* grown in Luria Bertani (LB) broth were evaluated and minimum inhibitory concentration (MIC) for each gel was determined.²⁵⁵ MIC is the lowest concentration of the selected component that renders no turbidity in bacterial culture corresponding to 99% of bacterial growth inhibition. To determine MIC of each gel 10 μ L bacterial culture having approximately 1×10^7 CFU/mL cells was added to 1 mL of LB. Various dilutions of the experimental gels were added to the tubes containing the bacterial cells and was incubated overnight. Next day, the MIC value was obtained by testing the turbidity of the bacterial culture.

3. RESULTS AND DISCUSSION.

3.1. Manifestation of ternary-phase diagram. Gibbs ternary phase diagram (Figure 1) studies demonstrate the occurrence of gel, viscous, precipitate and clear fluid states. With increasing proportion of HTAB, mixed aggregates form gel where the relative proportion of viscous and gel states increase that follow the order: $C_{12}MalNa_2 > C_{12}AspNa_2 > C_{12}GluNa_2$ (Figure 2) and data was shown in Table 1. Hydrophobic interaction between $(C_{12}AAS)Na_2$ and HTAB is the predominant factor for the formation of different types of aggregates besides the electrostatic attraction.¹⁷⁷ Carboxylate groups of $(C_{12}AAS)Na_2$ interact with HTAB at 2:1 ratio and form gel state at equimolar region due to the dominance of HTAB molecule.¹²³ Microstructural investigations on the gelatinous aggregates were further investigated through POM, FM and FE-SEM studies.

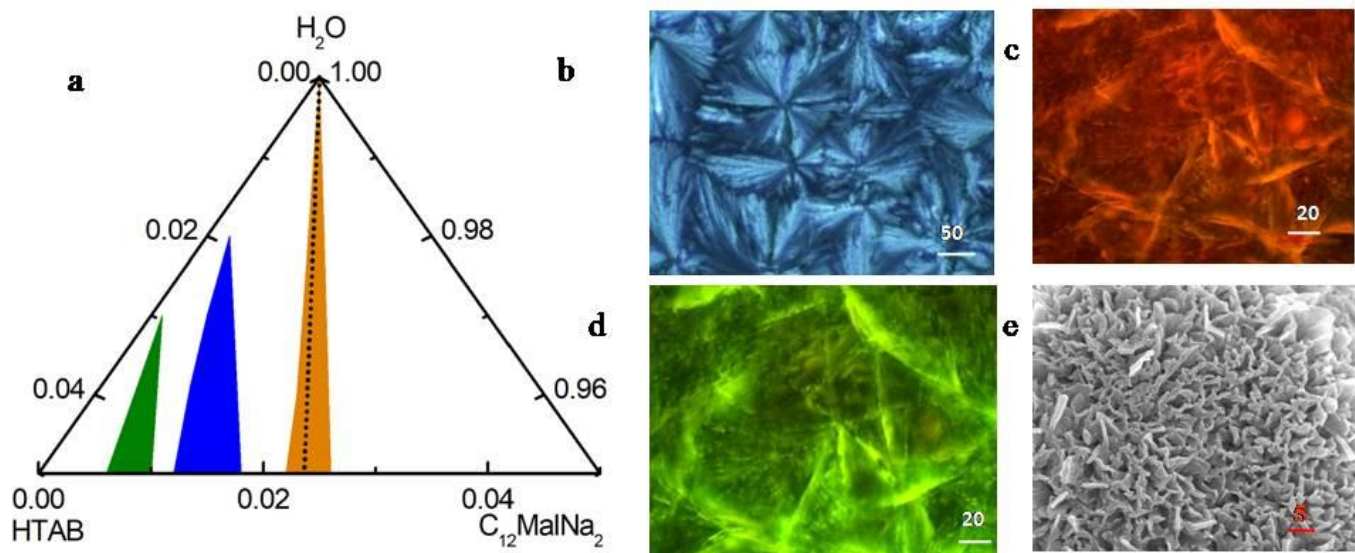


Figure 1. a, Truncated phase diagram of $C_{12}MalNa_2+HTAB+water$ mixed system. Phases: **olive**, gel; **blue**, viscous; **orange**, precipitate; and clear region indicate micelle. Dotted line in panel b corresponds to equimolar region. Panel b, POM image; c and d, FM images of rhodamine-B and fluorescein stained 5 wt% $C_{12}MalNa_2+HTAB$ (40:60, w/w) gel. Panel f, FE-SEM image of same gel.

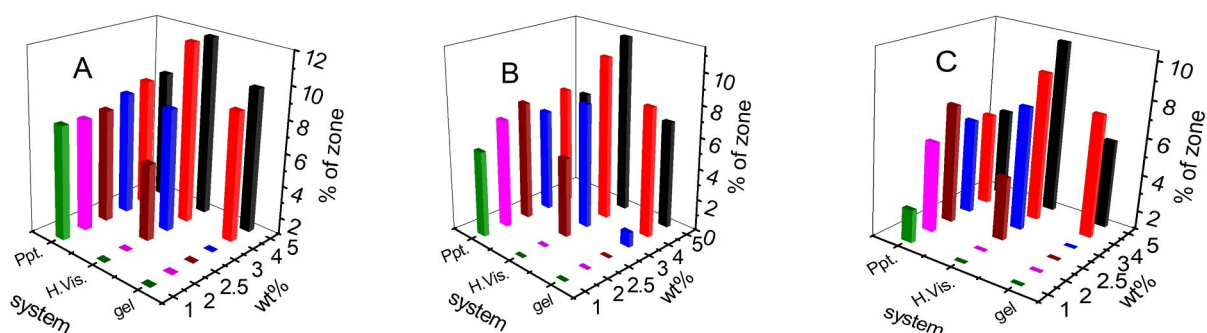


Figure 2. Variation of precipitation, highly viscous and gel of the ($C_{12}MalNa_2+HTAB$, panel A), ($C_{12}AspNa_2+HTAB$, panel B) and ($C_{12}GluNa_2+HTAB$, panel C) at different weight % at 298K.

3.2. Polarizing optical microscopy (POM) studies. POM studies reveal the occurrence of liquid crystal and associated textures as shown in (Figure 1c). Gels exhibit similar textures in the surfactant concentration range of 3 - 5 wt%. With increasing proportion of HTAB, $C_{12}MalNa_2$ gels display nematic, smectic, spherulite, cholesteric, calamitic, and flower like textures (Figure 3, Table 2).^{123, 256-258} The patterns become more complex with enhanced sizes due to the aggregation and associative interaction between ($C_{12}AAS$) Na_2 and HTAB. Texture size increases with increasing proportion of HTAB which has higher cross sectional area than the ($C_{12}AAS$) Na_2 .²⁰³ Features become more prominent with increasing mixed surfactant concentration, common in case of lyotropic liquid crystals (Figure 3).^{131,258} In case of

$C_{12}AspNa_2$ gels for 50, 60 and 80 wt% HTAB smectic, spherulite, and flower like patterns are observed,^{259, 260} while in case of $C_{12}GluNa_2$ discotic, lyotropic and flower like textures are predominant (Figure 4).

Table 1. Composition of different phases obtained for $(C_{12}AAS)Na_2/HTAB/H_2O$ system at 298K.

Composition of different phases	weight%								
	1	1.5	2	2.5	3	3.5	4	4.5	5
$C_{12}MalNa_2 / HTAB / H_2O$									
Gel	0.00	0.00	0.00	0.00	0.90	4.00	9.70	8.80	8.50
Viscous	0.00	0.00	0.00	5.60	8.40	9.60	11.9	11.9	12.9
Precipitation	7.80	5.60	7.70	7.80	8.40	8.00	8.90	8.80	8.50
Clear fluid	92.2	94.5	92.3	86.6	82.2	78.4	69.5	70.5	70.1
$C_{12}AspNa_2 / HTAB / H_2O$									
Gel	0.00	0.00	0.00	0.00	0.90	3.20	8.20	7.50	6.80
Viscous	0.00	0.00	0.00	5.00	7.90	8.00	10.4	10.0	11.3
Precipitation	5.40	4.70	6.90	7.50	6.50	6.40	7.50	6.90	6.80
Clear fluid	94.6	95.3	93.1	87.5	84.7	82.4	73.9	75.6	75.1
$C_{12}GluNa_2 / HTAB / H_2O$									
Gel	0.00	0.00	0.00	0.00	0.70	2.40	7.50	6.90	5.70
Viscous	0.00	0.00	0.00	4.30	7.50	6.40	8.90	8.80	10.2
Precipitation	2.70	3.80	5.70	7.20	6.10	5.60	5.90	5.70	2.00
Clear fluid	97.3	96.2	94.3	92.8	85.8	85.6	77.7	78.6	82.2

Two carboxylate groups of $(C_{12}AAS)Na_2$ are alienated by methylene group while moving from $C_{12}MalNa_2$ to $C_{12}AspNa_2$ to $C_{12}GluNa_2$. Accordingly, two carboxylate groups in $(C_{12}AAS)Na_2$ can electrostatically interact with one HTAB to form six, seven and eight member rings.²⁰³ Smectic textures designate ordered and rigid layer structure whereby $C_{12}MalNa_2$ can closely interact with HTAB to exhibit smectic texture. The nematic texture is characteristic of stacked layer and positional order whereby the discotic texture is due to rigid disk like core.^{261,262} $C_{12}MalNa_2$ gels display more prominent spherulite texture than $C_{12}AspNa_2$ due to the strongly aggregated structure and associative interaction between $(C_{12}AAS)Na_2$ and HTAB. $C_{12}AspNa_2$ and $C_{12}GluNa_2$ gels exhibit cholesteric texture because formation of sterically favourable seven and eight member rings (Figure 3a₄ and c₄). Columnar textures have relatively flexible core, exhibited by $C_{12}GluNa_2$ due to weak hydrophobic interaction.

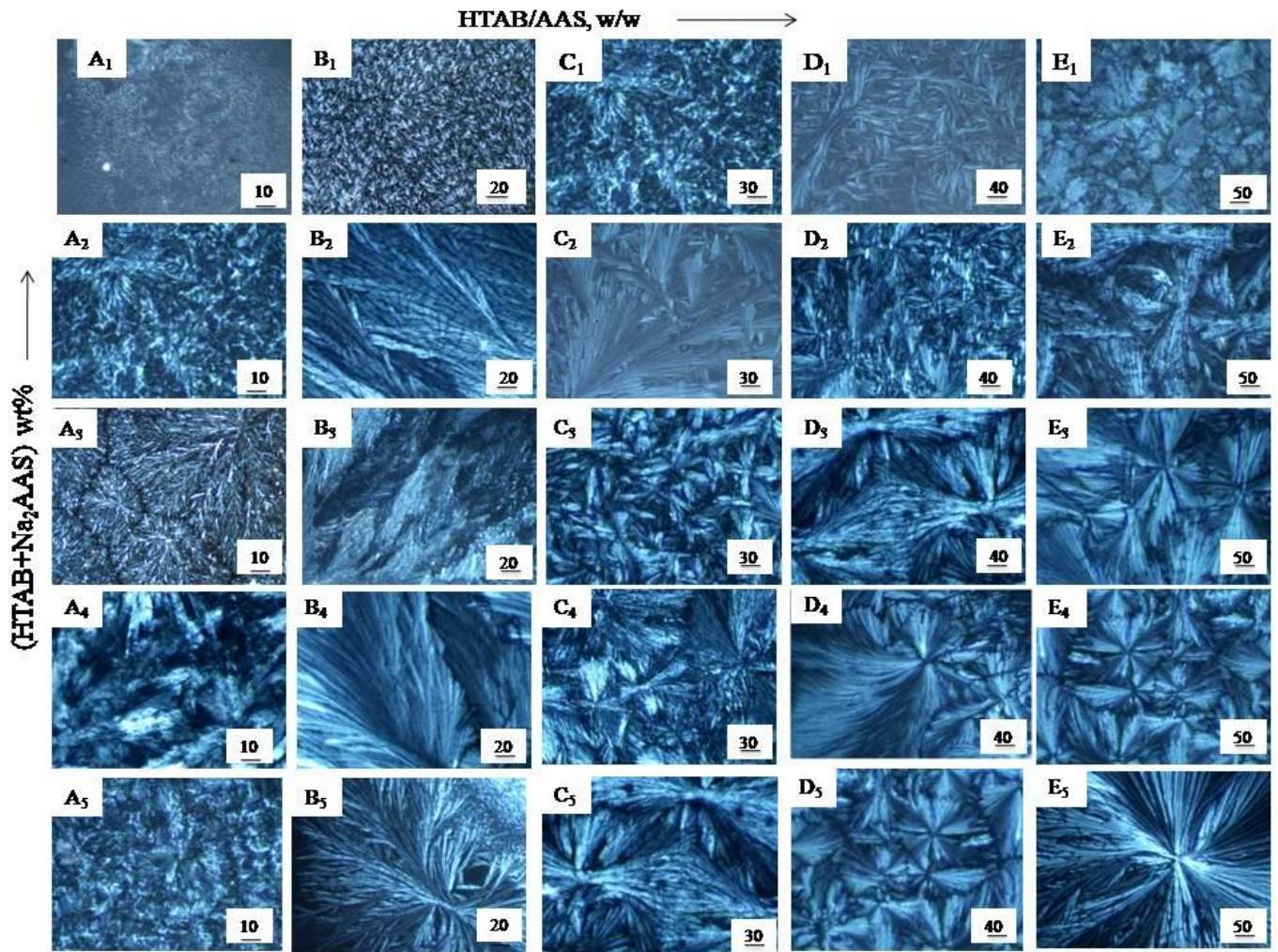


Figure 3. POM images of $C_{12}MalNa_2+HTAB$ at different compositions. Y axis: $(HTAB+(C_{12}AAS)Na_2)$ wt%; X axis: $HTAB/(C_{12}AAS)Na_2$, w/w. A_1, A_2, A_3, A_4, A_5 : 1, 2, 3, 4, 5; A_1, B_1, C_1, D_1, E_1 : 4/1, 3/2, 1/1, 2/3, 1/4. Scale bar are shown inside the images at 298K.

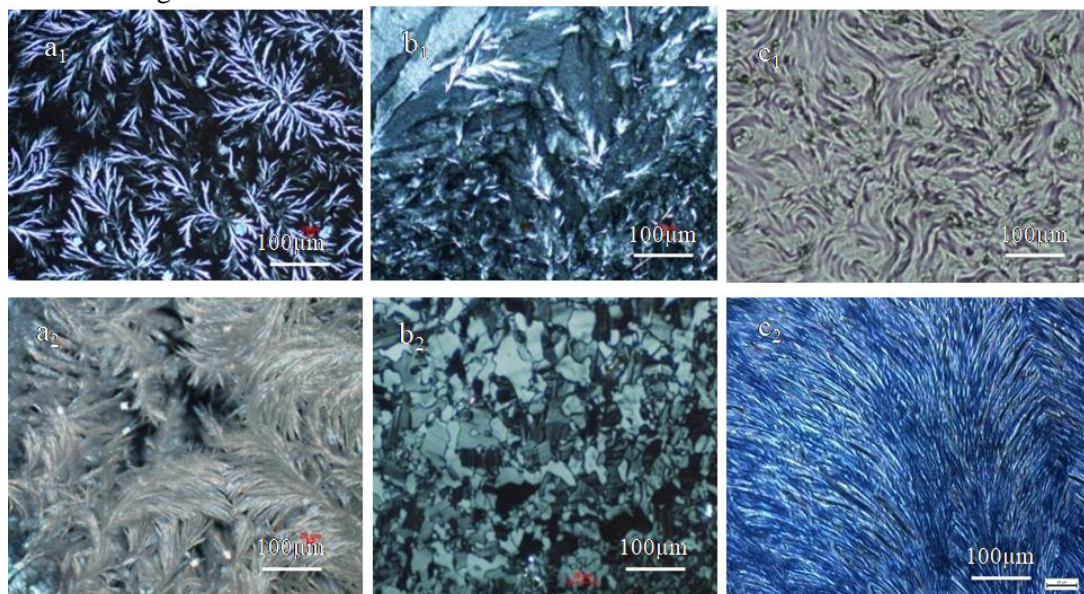


Figure 4. POM images $C_{12}AspNa_2+HTAB$ and $C_{12}GluNa_2+HTAB$ at different composition. Y axis: $(HTAB+(C_{12}AAS)Na_2)$ wt%; X axis: $HTAB/(C_{12}AAS)Na_2$, w/w. A_1, A_2 : 5; A_1, B_1, C_1 : 1/1, 3/2, 4/1. Scale bar are shown inside the figure at 298K.

3.3. Fluorescence microscopic (FM) studies. FM studies display fluorescence active liquid texture. Rhodamine-B and fluorescein were used as cationic and anionic dyes for FM studies. Rhodamine-B shows red fluorescence and binds to the anionic rich sites of the gels (Figure 1d).^{263, 264} Carboxylate groups of (C₁₂AAS)Na₂ interact with HTAB molecules where the systems are mostly anionic with lower proportion of HTAB. Fluorescein shows green fluorescence due to its binding with the cationic rich sites in liquid crystals (Figure 1e). However, when two dyes are mixed; no specific fluorescence is observed due to the mutual quenching between the dye molecules.²⁶⁵ Fluorescein weakly interacts with the anion rich mixed surfactants, hence fluorescence is not as strong as rhodamine-B. The prominent fluorescence patterns could be correlated with the textures as observed by POM studies, thus considered to be an alternative method.

3.4. Field emission scanning electronic microscopy (FE-SEM) studies. Microstructures of the aggregates were further investigated by FE-SEM studies which display interconnected morphologies (Figure 1f).^{140, 191, 265} With increasing proportion of HTAB, C₁₂MalNa₂ gels display rolled, wrinkled, cloth, coral, sponge, porous, and flower like morphologies schematically shown in Figure 5 and data was shown in Table 2.^{140, 266, 267} In case of C₁₂AspNa₂, gels with 50, 60 and 80 wt% of HTAB exhibit fiber, wrinkled and spheroid structures. For C₁₂GluNa₂, exposed honeycomb, snowball like microsphere and cloth like intertwined textures are prominent (Figure 6).^{129, 140, 241, 266, 267} C₁₂MalNa₂, in combination with HTAB show flower and coral like morphologies (Figure 6a₂). Even at higher magnifications, gels display non-porous morphology. C₁₂AspNa₂ and C₁₂GluNa₂ gels show characteristic honeycomb like morphology (Figure 6b₃) due to the emergence of micropores at the surface of gels.²⁶⁸ Clumped and spheroid texture of C₁₂MalNa₂ indicate extended sheet like feature and larger bundle fiber network structure. C₁₂AspNa₂ and C₁₂GluNa₂ gels have fiber network like morphology that can hold water molecules due to assisted its higher surface tension (Figure 6a₂ and b₃). Rolled, wrinkled, and sponge like architectures are due to the existence of protrusions and larger channels for which C₁₂MalNa₂ exhibit compact bundle fiber network morphology (Figure 5a₅ and b₄).²⁶⁷

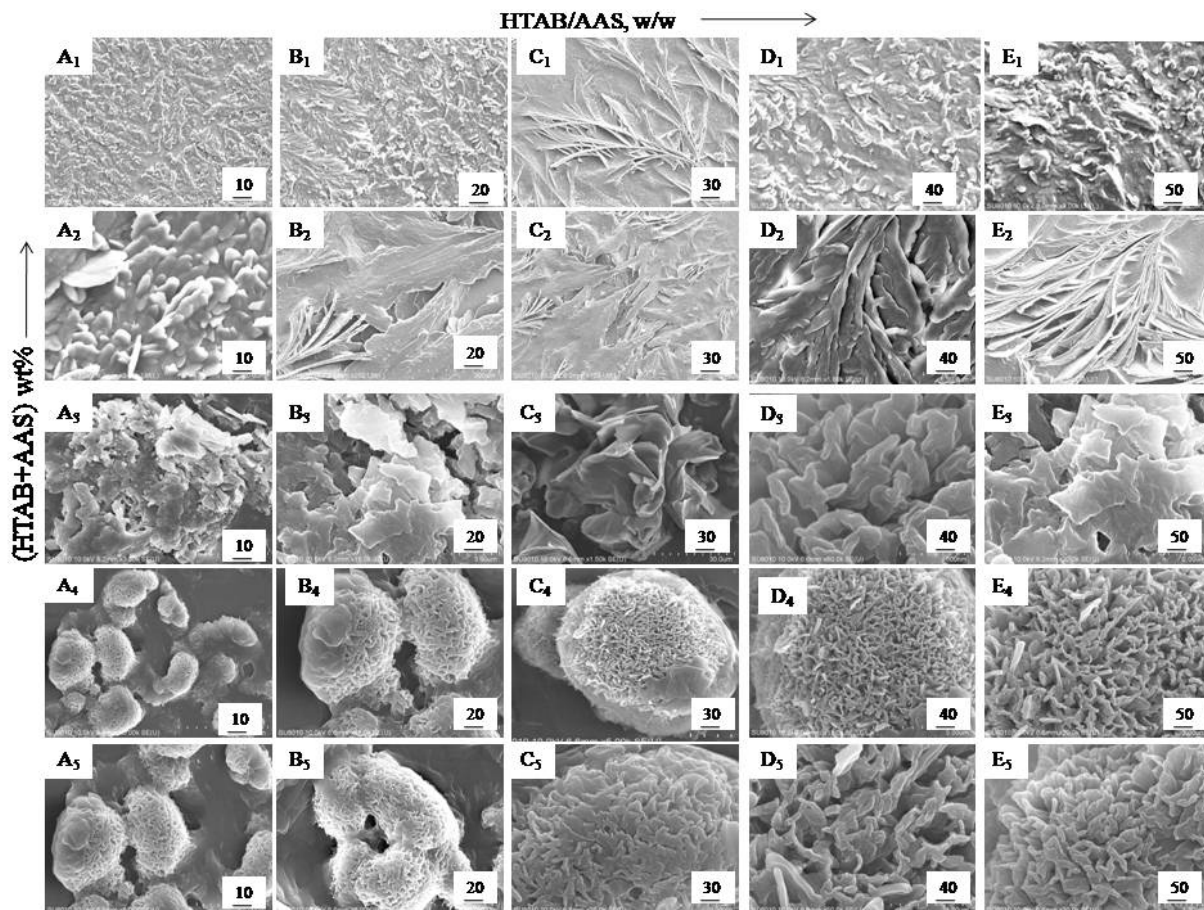


Figure 5. FE-SEM images of $C_{12}MalNa_2+HTAB$ at different compositions. Y axis: $(HTAB+(C_{12}AAS)Na_2)$ wt. %; X axis: $HTAB/(C_{12}AAS)Na_2$, w/w. A_1, A_2, A_3, A_4, A_5 : 1, 2, 3, 4, 5; A_1, B_1, C_1, D_1, E_1 : 4/1, 3/2, 1/1, 2/3, 1/4. Scale bar are shown inside the figure at 298K.

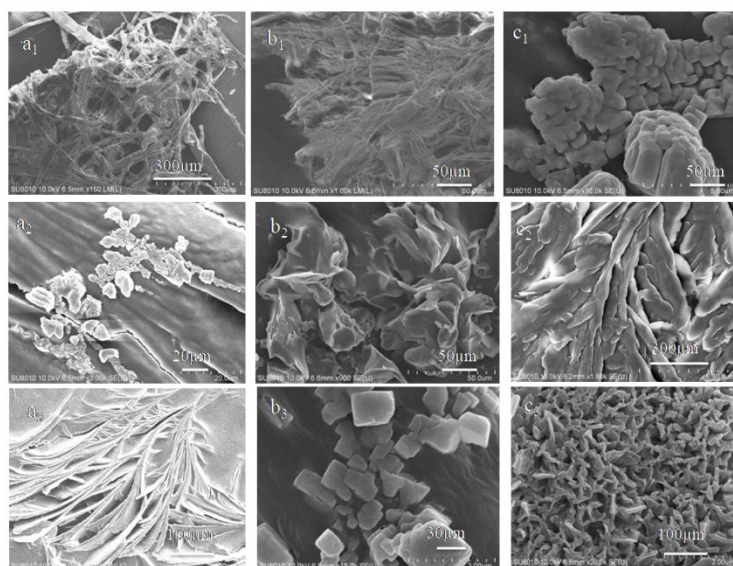


Figure 6. FE-SEM images of $C_{12}MalNa_2+HTAB$, $C_{12}AspNa_2+HTAB$ and $C_{12}GluNa_2+HTAB$ at different composition. Y axis: $(HTAB+(C_{12}AAS)Na_2)$ wt%; X axis: $HTAB/(C_{12}AAS)Na_2$, w/w. A_1, A_2 and A_3 : 5; A_1, B_1, C_1 : 1/1, 3/2, 4/1. Scale bar in μm are shown inside the figure at 298K.

Snowball and wrinkled morphologies in case of $C_{12}AspNa_2$ and $C_{12}GluNa_2$ indicate the entrapment of water molecules into the gels. Maximum number of HTAB molecule accumulates in gels that indicating HTAB plays fundamental role for higher aggregation and formation of porous like morphology, which are in consonance with the phase manifestation, POM and FM studies.

Table 2. POM and SEM image at different weight % of $(C_{12}AAS)Na_2+HTAB$.

		Phases				
$(HTAB+(C_{12}AAS)Na_2)$ wt%		$HTAB/(C_{12}AAS)Na_2$ (w/w)				
		20	40	50	60	80
1		nematic	smectic	columnar	rod	disk
2		calamitic	nematic	smectic	columnar	flower
3		nematic	spherulite	cholesteric	flower	flower
4		spherulite	texture weakly	calamitic	flower	flower
5		spherulite	flower	calamitic	flower	flower
		SEM (morphology)				
1		rolled	wrinkled	wet	cloth	coral
2		wrinkled	ribbon	fiber	sponge	flower
3		pumice	snowball	flower	fiber	flower
4		porous	flower	clumped	sponge	flower
5		pumice	flower	flower	flower	flower
		Phases				
$(HTAB+(C_{12}AAS)Na_2)$ wt%		$HTAB/(C_{12}AAS)Na_2$ (w/w)				
		20	40	50	60	80
1		nematic	smectic	columnar	rod	disk
2		calamitic	nematic	smectic	columnar	flower
3		nematic	spherulite	cholesteric	flower	flower
4		spherulite	texture weakly	calamitic	flower	flower
5		spherulite	flower	calamitic	flower	flower
		SEM (morphology)				
1		rolled	wrinkled	wet	cloth	coral
2		wrinkled	ribbon	fiber	sponge	flower
3		pumice	snowball	flower	fiber	flower
4		porous	flower	clumped	sponge	flower
5		pumice	flower	flower	flower	flower

3.5. Thermogravimetric analysis (TGA) studies. Phase transition and associated weight loss of gels were investigated by TGA studies.²⁶⁹⁻²⁷¹ Results on the thermogravimetric analysis of the pure components as well as $(C_{12}AAS)Na_2+HTAB$ aggregates have been summarized in (Figure 7 and Table 3).

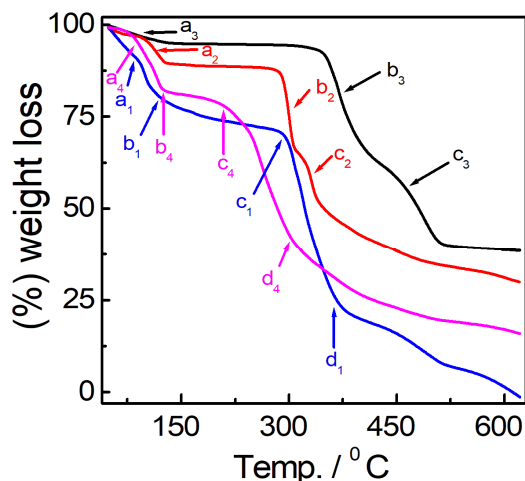


Figure 7. TGA thermogram of $(C_{12}AAS)Na_2$ and HTAB. System: blue; $C_{12}MalNa_2$, red; $C_{12}AspNa_2$, black; $C_{12}GluNa_2$, and magenta; HTAB where $a_1, b_1, c_1, d_1, a_2, b_2, c_2, a_3, b_3, c_3, a_4, b_4$ and c_4 represent the different phase transitions. Scan rate $2^\circ C \text{ min}^{-1}$.

Table 3. Results on the thermogravimetric analysis of pure and $(C_{12}AAS)Na_2+HTAB$ mixed gels system. Concentration: (100mM, $(C_{12}AAS)Na_2:HTAB = 40:60, M/M$).

Surfactant	Temperature range/ $^\circ C$	% wt. remaining
$C_{12}MalNa_2$	80-105	89
	105-186	79
	247-310	68
	351-412	25
$C_{12}AspNa_2$	86-125	93
	260-310	77
	310-345	51
$C_{12}GluNa_2$	73-123	96
	330-406	82
	422-508	55
HTAB	51-120	94
	113-158	81
	185-263	77
	294-360	41
$C_{12}MalNa_2+HTAB$	43-102	67
	232-259	27
$C_{12}AspNa_2+HTAB$	69-120	66
	268-300	18
$C_{12}GluNa_2+HTAB$	43-109	81
	119-288	63

HTAB decomposes to produce some solid carbon along with the production of long chain hydrocarbon, nitrogen, and hydrogen,^{269,272} whereby decomposition of $C_{12}MalNa_2$, $C_{12}AspNa_2$ and $C_{12}GluNa_2$ to produce dodecane (or smaller alkyl fragments) and amino-malonic,-aspartic and -glutamic acid.²⁷¹ Gels can be showed endothermic peaks in the temperature range of 40 to $100^\circ C$ due to the dehydration decomposition (Figure 8a).²⁷³

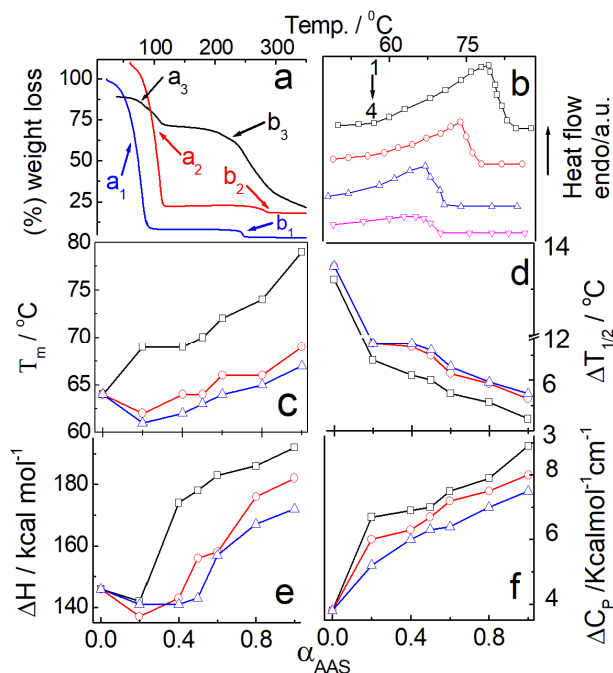


Figure 8. TGA thermogram of $(C_{12}AAS)Na_2+HTAB$ (100mM, 40/60, M/M) gel. Systems: blue; $C_{12}MalNa_2+HTAB$, black; red; $C_{12}AspNa_2+HTAB$ and $C_{12}GluNa_2+HTAB$. a_1 , b_1 , a_2 , b_2 , a_3 , and b_3 represent different phase transitions. (b), DSC thermogram of $C_{12}MalNa_2+HTAB$ mixture at different mole% of $C_{12}MalNa_2$: 1; 80, 2; 60, 3; 40, and 4; 0. Variation of (c), T_m ; (d), $\Delta T_{1/2}$; (e), ΔH and (f), ΔC_p with the mole fraction of $(C_{12}AAS)Na_2$ ($\alpha_{(C_{12}AAS)_2M_2}$). Systems: \square ; $C_{12}MalNa_2+HTAB$, \circ ; $C_{12}AspNa_2+HTAB$ and \triangle ; $C_{12}GluNa_2+HTAB$.

Two carboxylate groups of $C_{12}MalNa_2$ are hydrophobically interacted with HTAB results higher ionicity and subsequent moisture absorption capability than $C_{12}AspNa_2$ and $C_{12}GluNa_2$. In case of $C_{12}GluNa_2$, two ionic carboxylate groups are separated by two methylene groups so the interaction capability and magnitude of hydration is lower. In case formation of rigid aggregates result in the higher chain melting temperature (T_m) comparable with DSC studies.

3.6. Differential scanning calorimetry (DSC) studies. Thermotropic behavior and associated parameters were evaluated by DSC studies.¹²³ Variation of phase transition temperature (T_m), width at half peak height ($\Delta T_{1/2}$), enthalpy change (ΔH) and corresponding heat capacity change (ΔC_p) were determined as function of the surfactant composition (mole fraction of $(C_{12}AAS)Na_2$, $\alpha_{(C_{12}AAS)_2Na_2}$) as summarized in (Fig. 8) and data was shown in Table 4. HTAB exhibits two endothermic peaks at 64°C and 84°C due to the dehydration, as well as,¹²³ $(C_{12}AAS)Na_2+HTAB$ aggregates appear in the temperature range of 60-85°C (Figure 8b) because transition from solid-liquid crystalline phase and melting of the aggregates.²⁷¹ With increasing $\alpha_{(C_{12}AAS)_2Na_2}$, T_m values increases due to the incorporation of HTAB in the aggregates and assimilation of HTAB with the $(C_{12}AAS)Na_2$, relatively sharp peaks

appear indicating stronger of the hydrocarbon chain packing (Figure 8c).²⁰³ Lowering of T_m is due to size reduction, decreased specific surface area and interaction between oppositely charge surfactants also known as Kelvin effect.²⁷⁴ T_m values indicate that widening of the peaks that designate multi-crystallinity and heterogeneity. The extent of hydrophobic interaction between $(C_{12}AAS)Na_2$ and HTAB is lower in $C_{12}AspNa_2$ and $C_{12}GluNa_2$ than $C_{12}MalNa_2$ henceforth T_m values follow the sequence: $C_{12}MalNa_2 > C_{12}AspNa_2 > C_{12}GluNa_2$. With increasing $\alpha_{(C_{12}AAS)_2Na_2}$, $\Delta T_{1/2}$ values decrease indicating better packing of the hydrophilic over layer and hydrophobic interaction between oppositely charged head groups (Figure 8d). With increasing associative interaction between $(C_{12}AAS)Na_2$ and HTAB increased crystal imperfection results in the higher $\Delta T_{1/2}$ values. With increasing $\alpha_{(C_{12}AAS)_2Na_2}$, ΔCp value gradually increases and exhibits the endothermic peak due to the formation of water over layer around the surfactant aggregates (Figure 8f). Lower values of ΔCp are due to the increase in multicrystallinity.

Table 4. Differential scanning calorimetric data for the interaction of $(C_{12}AAS)Na_2$ with HTAB mixed surfactant system.

System	$T_m/ ^\circ C$	$\Delta T_{1/2}/ ^\circ C$	$\Delta H/kcal\ mol^{-1}$	$\Delta Cp/ kcal\ mol^{-1}C^{-1}$
$\alpha_{(C_{12}AAS)_2Na_2}$				
$C_{12}MalNa_2 + HTAB$				
1.0	79	3.7	192	8.9
0.8	74	4.7	186	7.9
0.6	72	5.2	183	7.5
0.5	70	6.0	178	7.0
0.4	69	6.3	174	6.9
0.2	69	7.2	142	6.7
0.1	64	13.2	146	3.8
$C_{12}AspNa_2 + HTAB$				
1.0	69	4.9	182	8.0
0.8	66	5.8	176	7.5
0.6	65	6.4	158	7.2
0.5	64	7.5	156	6.7
0.4	63	8.0	143	6.3
0.2	62	8.20	137	6.0
$C_{12}GluNa_2 + HTAB$				
1.0	67	5.2	172	7.5
0.8	65	5.9	167	7.0
0.6	64	6.8	157	6.4
0.5	63	7.8	143	6.3
0.4	62	8.2	141	6.0
0.2	61	8.2	141	5.2

3.7. Rheology studies. Viscosity studies on $(C_{12}AAS)Na_2+HTAB$ mixtures at different combinations exhibit shear thinning.²⁰³ Zero shear viscosity (η_0) vs. concentration profile for the gels comprising 60 mol% HTAB are shown in (Figure 9a).

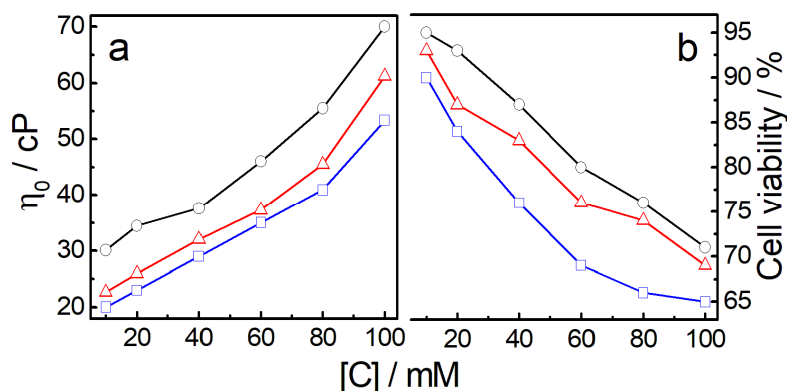


Figure 9. Variation of a, zero share viscosity and b, human blood lymphocyte cell viability with $(C_{12}AAS)Na_2 + HTAB$ (2/3, M/M) mixed surfactant concentration [C]. Systems: \circ , $C_{12}MalNa_2 + HTAB$; Δ , $C_{12}AspNa_2 + HTAB$; and \square ; $C_{12}GluNa_2 + HTAB$.

With increasing surfactant concentration viscosity increases monotonously in the range 10 to 100 mM. The sequence in the viscosity variation follow the order $C_{12}MalNa_2 > C_{12}AspNa_2 > C_{12}GluNa_2$, which are in consonance with the previous studies. Due to the stronger packing and subsequent formation of rigid structured aggregates viscosity of the $C_{12}MalNa_2$ system is higher than the other two.

3.2. Biological activities.

3.2.1. Cytotoxicity analyses of synthetic gel compounds. $(C_{12}AAS)Na_2+HTAB$ aggregate exhibit insignificant toxicity against human blood lymphocyte up to 20 mM; however, it increases with increasing surfactant concentration (Figure 9b). Cytotoxicities are in consonance with the corresponding viscosity of the mixtures.

3.2.3. Cutaneous irritation test. Gels do not exhibit symptom of cutaneous irritation and inflammation (erythema, edema, skin thinning and neutrophilic invasion) on the dorsal area of the trunk region of mice, similar to the effect of sterile distilled water used as negative control, unlike 5% phenol water (positive control) that causes redness and thinning of skin (Figure 4a-c).

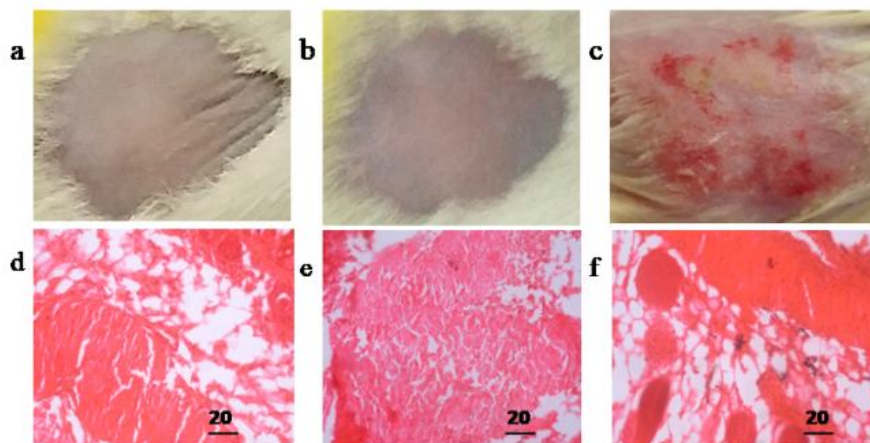


Figure 10. Skin irritation (a, b, c) and histological (d, e, f) tests on the dorsal area of trunk region of swiss albino mice. a and d, negative control (mice were treated with sterile distilled water); c and f, positive control (mice treated with 5% phenol-water; b and e, mice were treated with C₁₂MalNa₂+HTAB gel (100mM, 60/40 M/M).

3.2.4. Histopathological studies. Histological studies of Haematoxyline and eosin stained skins treated with gels, sterile water and 5% phenol respectively. Histological studies were performed to further visualize the presence of any inflammatory response (Figure 10d-f).²⁷⁵ Neutrophil infiltration and aggregation could only be found in the phenol treated skins, unlike the gel-treated and water (negative control) groups where no neutrophil invasion was observed. Results suggest that the gels can safely be used for topical applications.

3.2.5. Antibacterial activity. Gels also possess substantial antibacterial activity against *Staphylococcus aureus* pathogenic bacteria. In spite of about 90% lymphocyte viability, at 20 mM ((C₁₂AAS)Na₂:HTAB, 40:60, M/M) the surfactant mixtures are capable to cease bacterial growth (considered to be the MIC value).²⁵¹ The gels therefore can potentially be used in the treatment of bacteria born dermatological infections. Also the gels are expected to exhibit higher entrapment efficiency and sustained release of dermatological drugs. However, further *in vitro* and *in vivo* studies are warranted to substantiate the potential as drug delivery systems.

4. Summary and Conclusions

Micro-structures of $(C_{12}AAS)Na_2+HTAB$ aggregates were investigated by combined phase manifestation, optical and electron microscopic studies. Texture of the liquid crystals formed by the surfactant aggregates depend on the concentration and composition. Energetics of phase transition processes were evaluated by TGA and DSC studies. Cytotoxicity could be correlated with the viscosity of the gels. Gels impart insignificant skin irritation although they possess substantial antibacterial activities that project its potential as dermal drug delivery systems. However further *in vitro* and *in vivo* studies by incorporating appropriate drugs into the gels are necessary and being considered as the future perspectives.